Wearable integrated piezoelectric film sensor with tensioning, bending, shearing and twisting detection functions for human motion recognition

Lu Jin
The University of Manchester
Zhenhong Li
University of Leeds
Zekun Liu
The University of Manchester
Bethany Richardson
The University of Manchester
Yan Zheng
The University of Manchester
Lulu Xu
The University of Manchester
Zhongda Chen
The University of Manchester
Heng Zhai
The University of Manchester
Hongdoo Kim
Kyung Hee University
Qingwen Song
Xi'an Polytechnic University
Pengfei Yue
Xi'an Polytechnic University
Sheng Q. Xie
University of Leeds
Kap Jin Kim
Kyung Hee University
Yi Li (henry.yili@manchester.ac.uk)
The University of Manchester

Article

Keywords: Human-machine Interaction, Biomedical Engineering, Individual Joint Motion, Sensor Deformation, Poly L-lactic Acid Films

Posted Date: March 31st, 2021

DOI: https://doi.org/10.21203/rs.3.rs-290951/v1

Version of Record: A version of this preprint was published at npj Flexible Electronics on August 17th, 2022. See the published version at https://doi.org/10.1038/s41528-022-00205-4.

Wearable integrated piezoelectric film sensor with tensioning, bending, shearing and twisting detection functions for human motion recognition

Lu Jin[1], Zhenhong Li[2], Zekun Liu[1], Bethany Richardson[1], Yan Zheng[1], Lulu Xu[1], Zhongda Chen[1], Heng Zhai[1], Hongdoo Kim[3], Qingwen Song[4], Pengfei Yue[4], Sheng Q. Xie[2*], Kap Jin Kim[3*] and Yi Li[1,4*]

[1]Department of Materials, School of Natural Sciences, The University of Manchester, Manchester, M13 9PL, U.K.

[2]School of Electronic and Electrical Engineering, University of Leeds, Leeds, LS2 9JT, U.K.

[3]Department of Advanced Materials Engineering for Information and Electronics, Kyung Hee University, Yongin, 17104, South Korea

[4]College of Textile Science and Engineering, Xi'an Polytechnic University, Xi'an 710048, China

***Corresponding author:**

Yi Li (henry.yili@manchester.ac.uk)

Kap Jin Kim (kjkim@khu.ac.kr)

Sheng Q. Xie (S.Q.Xie@leeds.ac.uk)

Abstract

Human motion recognition using flexible/stretchable wearable sensors holds great promise for human-machine interaction and biomedical engineering. However, to measure the individual joint motion with multiple degrees of freedom, many sensor networks are normally required and pinpointed onto the targeted area, restricting body movement. This is due to the limitation of current wearable sensors; inferring a sensor deformation based on the sensor's electrical signal is challenging. A new concept of wearable sensor that can recognize how the sensor deforms could radically solve this issue. Here, we report a wearable integrated piezoelectric film sensor (i-PFS) capable of detecting basic deformations. To achieve this, for the first time, we propose a novel design concept of using uniaxially drawn piezoelectric poly L-lactic acid (PLLA) films to engineer unimodal tension, bend, shear, and twist sensors that only respond to their corresponding deformations with the enhanced piezoelectric response and self-shielding function. Based on this, we construct the i-PFS by combining the four unimodal sensors and demonstrate that the i-PFS can detect and differentiate individual deformation modes, such as tensioning, bending, shearing, and twisting. To our best knowledge, the i-PFS is the world's first film-based sensor that identifies the abovementioned deformations. To prove the potential impact of the i-PFS, we design a sleeve and a glove with the i-PFS that can capture various wrist motions and subtle finger movements, respectively. We also develop a virtual text-entry interface system using the glove and a deep neural network algorithm with

a character classification accuracy of ~ 90 %. The i-PFS technology is expected to provide a turning point in developing motion capture systems.

Human motion recognition is of great importance for human-machine interaction[1,2], entertainment[3,4], and rehabilitation[5,6]. Several techniques have been developed to measure human motions. One method utilizes the camera-based motion capture system to record a subject's detailed actions, but it requires high computational loads and limits activity range[7,8]. Another approach is to apply inertial sensors, but the sensors' rigidity confines their application in daily life[9,10]. Alternatively, flexible/stretchable, lightweight wearable sensors, such as piezoelectric sensors, resistive sensors, capacitive sensors, triboelectric sensors, and so forth, provide a promising way for motion monitoring[11–16]. However, the vast majority of human body joints have multiple degrees of freedom[17–19]. To identify the complicated individual joint motion precisely, multiple wearable sensors are required and pinpointed onto the desired positions, restricting the naturalness of movements[20–25]. Fundamentally, such inefficiency and impracticality are ascribed to the limitation of existing wearable sensors; gaining information on a sensor deformation from the sensor's electrical signal is a huge challenge. For instance, the wrist has multiple degrees of freedom; it can bend, twist, and even rotate[20]. We can detect an electrical signal from a sensor attached to the wrist joint once deformed. Conversely, it is not easy to infer the wrist deformation (i.e., the sensor deformation) based on the detected electrical signal because any wrist motion generates a signal. It is highly desirable to develop a new type of wearable sensor, which can provide

feedback on the sensor deformation, to radically solve the above problem.

Hence, we propose a novel concept of a wearable sensor comprising uniaxially drawn piezoelectric poly L-lactic acid (PLLA) films, i.e., an integrated piezoelectric film sensor (i-PFS), which can detect and differentiate four typical deformations, such as tensioning, bending, shearing, and twisting.

Theoretical background

To develop the i-PFS, we first design four unimodal tension, bend, shear, and twist sensors with the piezoelectric PLLA films, which only respond to tensioning, bending, shearing, and twisting, respectively. The pristine piezoelectric PLLA film only presents a shear piezoelectric coefficient (PC), i.e., d_{14}, because of its helical structure[26]. It is usually cut at a certain angle from the crystal orientation (i.e., drawing direction) of the original PLLA film to respond to an external stimulus via modifying its PC[27]. We, therefore, calculated PCs of four PLLA films with particular cutting angles (CA) such as 45°, -45°, 0°, and 90° through a mathematical model of the PCs of PLLA film. Of particular interest is that two normal PCs along with the width and length directions, i.e., d_{12} and d_{13}, are newly created in the PLLA films with CAs of 45° and -45°, named PLLA45 and PLLA-45; simultaneously, the primary shear PC, d_{14}, disappears. Besides, the two normal PCs of PLLA45 are opposite to those of PLLA-45. In contrast, the PLLA films with CAs of 0° and 90°, called PLLA0 and PLLA90, only have the shear PC, d_{14}; they are opposite each other as well (see Supplementary Note 1). We then analyzed the four PLLA films' piezoelectric responses when subjected to typical deformations, such as tensioning, bending, shearing, and twisting, via finite element

simulations using ABAQUS. As shown in the top schematic of Fig. 1a, the deformation directions of tensioning, bending, and shearing (i.e., applied force directions) in simulations cover three axes of a 3-D cartesian system. Notably, a more complex twisting deformation is considered in this work. Thus, these four basic deformation components will introduce any morphologic change to the PLLA film. The PLLA45 and PLLA-45 are sensitive to the tensioning and bending deformations because the average voltage of all nodes of each PLLA film surface (V_a) is non-zero. Moreover, the generated voltages of each sample are vertically symmetrical, but they are opposite under shearing or twisting and thus offset each other inside (i.e., $V_a = 0$), not showing a piezoelectric response on the whole. This is attributed to the normal PCs of the PLLA45 and PLLA-45. Similarly, the PLLA0 and PLLA90 are only responsive to the shearing and twisting deformations because of the shear PCs (Fig. 1a and Supplementary Video 1). Overall, each PLLA film is still sensitive to two deformation modes, indicating that it is impossible to determine the exact deformation status with the piezoelectric signal measured from the single-layer PLLA film sensor during deformation. Crucially, we find that the PLLA45 and PLLA-45 generate opposite voltages under the same deformation, and so do PLLA0 and PLLA90.

Design concept and hypothesis of unimodal sensors

Based on the above findings, we introduce a double-layer PLLA film design concept of unimodal tension, bend, twist, and shear sensors, as illustrated in Fig. 1b,c. We hypothesize that as the unimodal tension sensor consists of two PLLA45s, both receive tensile stress when tensioned, producing the same charges in the inner and outer

electrodes, respectively; the electric signals of two PLLA45s will be superimposed. Under bending, the upper area of each PLLA45 receives compressive stress, whereas the bottom area is relatively subjected to tensile stress, generating the opposite charges; the signals of two PLLA45s will be canceled out. The charges produced will also be offset inside each PLLA45 under twisting and shearing deformations, not showing signal, as illustrated in Supplementary Fig.2. Conversely, as the unimodal bend sensor is composed of PLLA45 and PLLA-45, the bend sensor's signal will be boosted under bending, but it will be offset when tensioned. To theoretically prove the design concept, the piezoelectric responses of both PLLA films of the unimodal tension, bend, twist, and shear sensors were simulated under different deformations. As long as the unimodal sensors receive their matched deformations, two PLLA films composing each unimodal sensor produce the same piezoelectricity; otherwise, they generate opposite voltages (Fig. 1d), which exactly agrees with our hypothesis.

Unimodal sensors fabrication and performance test

The piezoelectric property of uniaxially drawn PLLA film is strongly dependent on its crystal orientation and crystallinity, which are dominated by fabrication conditions, especially the drawing ratio (DR)[26,28]. We, therefore, prepared four uniaxially drawn piezoelectric PLLA films with different DRs, such as 3.3, 3.7, 4.0, and 4.5 (Fig. 2a). As shown in Fig. 2b, the crystal orientation improves with increasing the DR because a Debye-Scherrer ring displayed at an initial DR of 3.3 gradually becomes three ellipses at a maximum DR of 4.5, indicating the highly orientated α-crystal structure is formed[29]. This behavior is observed by their melting thermograms as well. After a glass transition

temperature (T_g= 64°C), the cold crystallization temperature (T_c) of the drawn PLLA films appears at different temperatures, and the lower DR, the higher T_c. This is because the low chain orientation of the PLLA film requires more energy to form the ordered arrangements and undergoes crystallization at a higher temperature (Fig. 2c). Besides, there is a single melting peak (T_m) at around 170 °C, a typical α-crystal melting peak[26], but the β-crystal melting peak at T_m= 155 °C is not observed[30], further confirming all PLLA films are only compose of α-crystal. The crystallinity increases with increasing the DR, and it reaches 60.9 % at a DR of 4.5 (Fig. 2d). As a result, the piezoelectric PLLA film with the DR of 4.5 exhibits the most superior piezoelectric response among them (Fig. 2e). Therefore, the PLLA film with the DR of 4.5 was selected and fabricated into four unimodal tension, bend, twist, and shear sensors following the proposed design concept (Fig. 2f). Notably, as the prepared PLLA film with α-crystal (i.e., 10_3 helical structure) does not present a remnant polarization prior to any shear deformation, one cannot determine its resultant polarization direction when it is shear-deformed without a measurement; in other words, which side of the PLLA film produces positive charges or negative charges when deformed. One, however, can hypothesize that the front sides of two PLLA45s and two PLLA0s certainly generate the same charges, whereas those of the PLLA45 and PLLA-45 and the PLLA0 and PLLA90 undoubtedly produce the opposite charges in the identical deformation because they are cut from the same PLLA film sheet. Therefore, to facilitate the process of sensor fabrication, the front sides of the two matched PLLA parts are stuck to each other.

These unimodal sensors were tested one by one under the tensioning, bending,

155 twisting, and shearing conditions. Comparing four unimodal sensors under the same
156 deformation condition (i.e., horizontal comparison of Fig. 3a), each sensor exhibits the
157 most significant piezoelectric behavior when received matched stimulus; otherwise,
158 almost no response (P-value < 0.001, Fig. 3b). To further evaluate their piezoelectric
159 behavior when subjected to different deformations, the corresponding peak to peak
160 signal amplitudes ($V_{p\text{-}p}$) of Fig. 3b are normalized (see Method) to compare all signals
161 under the same scale. As expected, all unimodal sensors are sensitive to their
162 corresponding deformations but insensitive to the other conditions (Fig. 3c). Besides,
163 the unimodal sensors can identify the applied force direction (Fig. 3a and
164 Supplementary Fig. 3). We also evaluated the stability and repeatability of the unimodal
165 sensors. The stable and continuous piezoelectric response during 1000 cycles and the
166 reproduced piezoelectric signals after each day without significant variation
167 demonstrate signal stability and repeatability (Supplementary Fig. 4). The unimodal
168 tension sensor exhibits a relatively stronger piezoelectric noise signal than the other
169 sensors under unmatched deformations (Fig. 3c). This is ascribed to the mismatching
170 of two PLLA45s composing the tension sensor. The operating mechanism of these
171 sensors is amplifying their signals when subjected to the corresponding stimuli but
172 offsetting under unmatched deformations. The latter is a key for the unimodal sensors,
173 and it is much more difficult to be achieved than the former. This is because a slight
174 discordance in piezoelectric and physical properties of two PLLA films, such as CA,
175 drawing direction, size, and thickness, could result in a non-negligible noise signal even
176 under the non-corresponding stimuli. For instance, a slight deviation on the CA of the

177 PLLA45 can cause the residual shear piezoelectric coefficient, d_{14}, in the PLLA45,
178 which acts to shearing and twisting deformations. The size or thickness difference can
179 also lead to the uneven force receiving between two PLLA45s. To minimize such
180 discrepancies, the two PLLA parts of each unimodal sensor should be cut from the same
181 area of the original PLLA film, and the closer the two parts, the better the performance.
182 Another difficulty in the unimodal sensor fabrication is finding the exact uniaxial
183 drawing direction of the transparent PLLA film because an incorrect drawing direction
184 could lead to an inevitable error in the CA.

185 Fig. 3d compares the piezoelectric responses of the four unimodal sensors and
186 conventional PLLA film (single layer) sensors following the above conditions. Notably,
187 all unimodal sensors exhibit much higher piezoelectric responses than the PLLA
188 sensors under corresponding deformations, but their increased levels are different.
189 Under tensioning and shearing, the $V_{p\text{-}p}$ of the tension and shear sensors almost double
190 compared to the single PLLA film sensors. It is reasonable because the tension and
191 shear sensors consist of two PLLA films, producing coherent piezoelectric signals
192 under the corresponding deformation. For the bend sensor, its $V_{p\text{-}p}$ is twenty times
193 stronger than that of the PLLA45 sensor. Under the same bending curvature, the bend
194 sensor's two PLLA45 films should be subjected to more massive bending stress than
195 the PLLA45 sensor because of the thicker thickness. Thus it does not merely generate
196 a doubled signal but produces a much stronger signal than the PLLA45 sensor. Similarly,
197 the twist sensor presents a boosted piezoelectric behavior compared with the PLLA0
198 sensor; significantly, it shows about seventy times stronger signal than the PLLA0

sensor at a twisted angle of 30°. To further confirm this, we compared the $V_{p\text{-}p}$ of two sensors at twisted angles of 20° and 40°, which all show consistent results (Supplementary Fig. 5).

Owing to the capacitive feature of piezoelectric sensors, including the conventional piezoelectric PLLA sensor, they are quite susceptible to electromagnetic (EM) interference (e.g., 50 Hz EM noise originated from the household electricity) and motion artifact in a real-world setting[31]. It is easy to eliminate the 50 Hz EM noise using an appropriate electronic filter system because of the regular frequency. Conversely, most motion artifact caused by the human body has an irregular frequency; it could be challenging to be removed using a particular electronic filter system. Therefore, the piezoelectric sensors themselves should have a proper EM shielding function to apply for wearables. Since the outer electrode of each unimodal sensor covers the inner electrode completely and is connected to a metallic shield part of a coaxial cable (Fig. 1c), it can serve as an EM shielding layer. In contrast to the unshielded PLLA45 sensor, the self-shielded unimodal tension sensor exhibits excellent noise-screening performance against the 50 Hz EM noise and motion artifact (Fig. 3e and Supplementary Video 2). Besides, the PLLA film is quite vulnerable to moisture/water because of the biodegradable nature[28,32]. The outer electrode covers all outside surfaces of the sensors, seamlessly protecting the PLLA films from moisture/water. Nevertheless, for the applications of biodegradable sensors, their durability could also be adjustable by changing the outer electrode's property, e.g., biodegradable materials-based electrodes[5,28,33].

Integrated piezoelectric film sensor (i-PFS)

We then fabricate the i-PFS by stacking four unimodal sensors together, as shown in Fig. 3f. The i-PFS was tensioned, bent, twisted, and sheared using the relevant machines. The result proves that the i-PFS has enough capability to detect and differentiate tensioning, bending, twisting, and shearing deformations, respectively (Fig. 3f and Supplementary Fig. 6). More importantly, this demonstrates that the four unimodal sensors composing the i-PFS can work together without evident interference. This is mainly because the individual unimodal sensor is shielded by each outer electrode, not affecting each other. The i-PFS was also deformed by hand to investigate the practicability. As expected, the i-PFS can discriminate imposed motions separately, as shown in Supplementary Fig. 7 and Supplementary Video 3.

Motion recognition applications

Unlike most piezoelectrics, the piezoelectric PLLA film has no pyroelectricity, which means its signal is not influenced by temperature fluctuation[27], presenting the unique advantage of the i-PFS in real-life applications. To demonstrate the potential of the i-PFS in human motion recognition applications, we fabricated a sleeve with the i-PFS (i-Sleeve for short) to measure various wrist motions. Since the four unimodal sensors composing the i-PFS independently respond to their corresponding deformations (tensioning, bending, shearing, and twisting), the i-Sleeve can differentiate complex wrist motions involving multiple degrees of freedom (e.g., extension/flexion, radial/ulnar deviation, pronation/supination) as shown in Supplementary Fig. 8 and Supplementary Video 4. More importantly, a complicated wrist turning action

243 comprising three bending, twisting, and shearing deformation components is
244 simultaneously detected by the bend, twist, and shear sensor channels, respectively.
245 This further implies that the i-PFS could decouple complex human motions.
246 Supplementary Table 1 summarizes relevant works on wrist motion capture. The i-
247 Sleeve is unique as it does not require multiple sensors that are distributed to the desired
248 area. It utilizes a single i-PFS to further identify wrist turning action that is superior to
249 conventional approaches, showing the great efficiency of the i-PFS.

250 Furthermore, the i-PFS was integrated into an index finger of a glove (i-Glove for
251 short) to evaluate its performance in subtle motion detection (the bottom inset of Fig.
252 4a), i.e., index finger movements. Due to the limited surface area available on a finger,
253 it is challenging to attach multiple sensors. Therefore, most previous studies focused on
254 tracking the fingers' flexion and extension motion (Supplementary Table 2). It is still
255 an open issue to capture index finger movements involving multiple degrees of freedom
256 with wearable sensors. The i-PFS of the i-Glove can discriminate various finger modes,
257 such as bending up and down, shearing left and right, turning clockwise and anti-
258 clockwise, and flexion and extension (Fig. 4b). Besides, the i-PFS can distinguish the
259 finger movements' directions.

260 Based on this, we designed a virtual text-entry interface system using the i-Glove in
261 conjunction with a convolutional neural network (CNN) algorithm for a finger-air-
262 writing application, which detects finger movements with the i-PFS and transforms
263 them into corresponding characters (Fig. 4a,c and Supplementary Video 5). We chose
264 13 characters (i.e., "U", "O", "M", "0", "1", "2", "3", "4", "5", "6", "7", "8", "9") as

target classes. One participant was invited to create the data source for the finger-air-writing (see Method). As the character writing habit influences the output signal, the writing style of each character was defined before collecting data to eliminate its effect. For instance, we instructed the participant to write the letter "O" in clockwise and the number "0" in anti-clockwise to distinguish them. Supplementary Fig. 9 displays the output data of 13 characters of three trials, which shows good signal reproducibility. We then adopted a LeNet-5 based CNN architecture consisting of two convolutional layers for character classification (Supplementary Fig. 10). The classification result shows that the accuracy using four channels can reach 89.7 % (Fig. 4d). We also examined the classification accuracies of individual sensor channels, two and three-channel combinations. The results show that the testing accuracies increase with increasing the channel numbers; the mean classification accuracy can reach 85 % when using any three sensor channels (Supplementary Fig. 11-13). Several groups have exploited the vision-based system[7,8], the inertial sensors[34], and their combination[35] for air-writing implementation. Unlike these approaches, our finger-air-writing is realized merely using the wearable i-PFS to detect the subtle metacarpophalangeal joint movement of the index finger, demonstrating the performance of the i-PFS in minute motion monitoring.

Conclusion

In summary, we present a new type of wearable sensor, i.e., i-PFS, capable of identifying tensioning, bending, twisting, and shearing deformations and demonstrate the potential impact of the i-PFS in motion recognition systems. To realize this, four

unimodal sensors for the i-PFS are designed and fabricated by sticking two uniaxially drawn piezoelectric PLLA films with different CAs, endowing the sensors with the functions of not only detecting and differentiating unimodal deformations but also the self-shielding ability. These unimodal sensors and their combinations can be utilized as various film-based force, strain, and deformation sensors with 1, 2, or 3-axial sensitivity depending on the purpose. Significantly, the sensors will be incredibly beneficial in the applications of implantable and biodegradable sensors because of the excellent biocompatibility and biodegradability of the PLLA. We also expect that the novel design principle of unimodal piezoelectric sensors and i-PFS proposed here can be applied to other piezoelectrics, making them more powerful and smarter.

Methods

Piezoelectric response simulations of four uniaxially drawn piezoelectric PLLA films with various cutting angles under tensioning, bending, shearing, and twisting deformations

Parameters used for the piezoelectric response simulations are as follows: a PLLA piezoelectric coefficient (d_{14}) of 10×10^{-12} C/N, a PLLA density of 1250 kg/m^3, a PLLA Young modulus of 4×10^9 Pa, a PLLA Poisson's ratio of 0.36, and all parameters are estimated values based on the reference[36]. The dimension of the PLLA films (Length × Width × Thickness) is 2 × 1 × 0.01 cm. The applied forces for tensioning, bending, and shearing deformations are 1×10^4 Pa, 1×10^1 Pa, and 1×10^3 Pa, respectively. For twisting deformation, the PLLA film is vertically divided into two parts, and one part applies 1×10^3 Pa and the other part -1×10^3 Pa.

PLLA chips for uniaxially drawn piezoelectric PLLA film preparation

Ingeo biopolymer 4032D ($M_w \approx 195\,000$, NatureWorks, USA) with 98 % L-isomer and 2 % D-isomer was used for uniaxially drawn piezoelectric PLLA film preparation.

Output voltage measurement under tensioning, bending, shearing, and twisting deformations

The output voltages were acquired in the voltage mode of a Piezo Film Lab Amplifier (Measurement Specialties, Inc., USA) in a condition of an input impedance of 10 MΩ, a band-pass filter range of 0.1-10 Hz, and a gain value of 0 dB at 100 Hz of the sampling rate. For the shielding performance test, the input impedance and the band-pass filter range of the Piezo Film Lab Amplifier increase to 1 GΩ and 0.1-1000 Hz, respectively.

Tensioning deformation was realized using an electromechanical universal testing system (Instron, a strain of 1 %), and the other deformations were performed using a bending machine (a bending angle of 21.8°), a twisting machine (a twisted angle of 30°), and a shearing machine (a shear strain of 0.05) with a frequency of 0.5 Hz, as illustrated in Supplementary Fig. 14.

Characterizations of uniaxially drawn piezoelectric PLLA films

To determine the crystal orientation and crystallinity of the uniaxially drawn piezoelectric PLLA film, two-dimensional wide-angle x-ray diffraction (2D-WAXD) photograph and the corresponding 1D-WAXD spectrum were obtained in reflection mode using a Rigaku SmartLab 3K diffractometer with a Cu Kα (λ = 1.54 Å) radiation source ranging from 2θ = 4° to 40°. Crystallinity percentages of the PLLA films were quantified from the curve deconvolutions of their corresponding 1D-WAXD spectrums. The melting thermograms were measured utilizing a differential scanning calorimeter (DSC Q2000, TA Instruments, USA) at a heating rate of 10 °C/min from 40 to 190 °C at nitrogen atmosphere.

Unimodal sensors' signals normalization

To compare each unimodal sensor's piezoelectric response under different deformation conditions, its noise signal under unmatched conditions should be considered because it increases with increasing non-corresponding deformation degree/intensity. For example, under tensioning deformation, the signals recorded from the bend, twist, and shear sensors are regarded as noises; these noises certainly increase with increasing the tensioning intensity that is directly reflected by the tension sensor, as shown in Fig. 3b.

In other words, the noises increase with increasing the signal of the tension sensor. This causes big trouble in comparing each sensor's exact piezoelectric response under different deformations and their noise levels. To solve this problem, all $V_{\text{p-p}}$ of the sensors under each deformation condition are normalized by dividing the $V_{\text{p-p}}$ of the matched sensor under the same deformation (below equations) to place all signals on the same scale (0 ~ 1) as summarized in Fig. 3c.

$$\text{For tensioning: } V'_{p-p} = \left[\frac{V_{p-p}^{tension}}{V_{p-p}^{tension}}, \quad \frac{V_{p-p}^{bend}}{V_{p-p}^{tension}}, \quad \frac{V_{p-p}^{twist}}{V_{p-p}^{tension}}, \quad \frac{V_{p-p}^{shear}}{V_{p-p}^{tension}} \right]$$

$$\text{For bending: } V'_{p-p} = \left[\frac{V_{p-p}^{tension}}{V_{p-p}^{bend}}, \quad \frac{V_{p-p}^{bend}}{V_{p-p}^{bend}}, \quad \frac{V_{p-p}^{twist}}{V_{p-p}^{bend}}, \quad \frac{V_{p-p}^{shear}}{V_{p-p}^{bend}} \right]$$

$$\text{For twisting: } V'_{p-p} = \left[\frac{V_{p-p}^{tension}}{V_{p-p}^{twist}}, \quad \frac{V_{p-p}^{bend}}{V_{p-p}^{twist}}, \quad \frac{V_{p-p}^{twist}}{V_{p-p}^{twist}}, \quad \frac{V_{p-p}^{shear}}{V_{p-p}^{twist}} \right]$$

$$\text{For shearing: } V'_{p-p} = \left[\frac{V_{p-p}^{tension}}{V_{p-p}^{shear}}, \quad \frac{V_{p-p}^{bend}}{V_{p-p}^{shear}}, \quad \frac{V_{p-p}^{twist}}{V_{p-p}^{shear}}, \quad \frac{V_{p-p}^{shear}}{V_{p-p}^{shear}} \right]$$

where V'_{p-p} is the normalized $V_{\text{p-p}}$, $V_{p-p}^{tension}$ is the $V_{\text{p-p}}$ of the tension sensor under each deformation, V_{p-p}^{bend} is the $V_{\text{p-p}}$ of the bend sensor, V_{p-p}^{twist} is the $V_{\text{p-p}}$ of the twist sensor, and V_{p-p}^{shear} is the $V_{\text{p-p}}$ of the shear sensor.

Signal collection and process of the finger-air-writing

The participant is asked to perform 100 trials of air-writing wearing the i-Glove. In each test, the participant continuously writes the 13 characters using the index finger, and the writing time for each character is about 2 s. The output data of i-PFS from four channels are recorded at 100 Hz. The collected multi-channel data are then filtered digitally using a sixth-order low-pass Butterworth filter with a 10 Hz cut-off frequency and is segmented using a 1 s sliding window with 0.2 s increment. Since the spectrum

of output data from i-PFS is observed to be less noisy and more distinguishable than the output data in the temporal domain, each segmented data channel is applied for fast Fourier transform (FFT). The transformed data is split into 80 % and 20 % and used as a training set and test set of CNN, respectively.

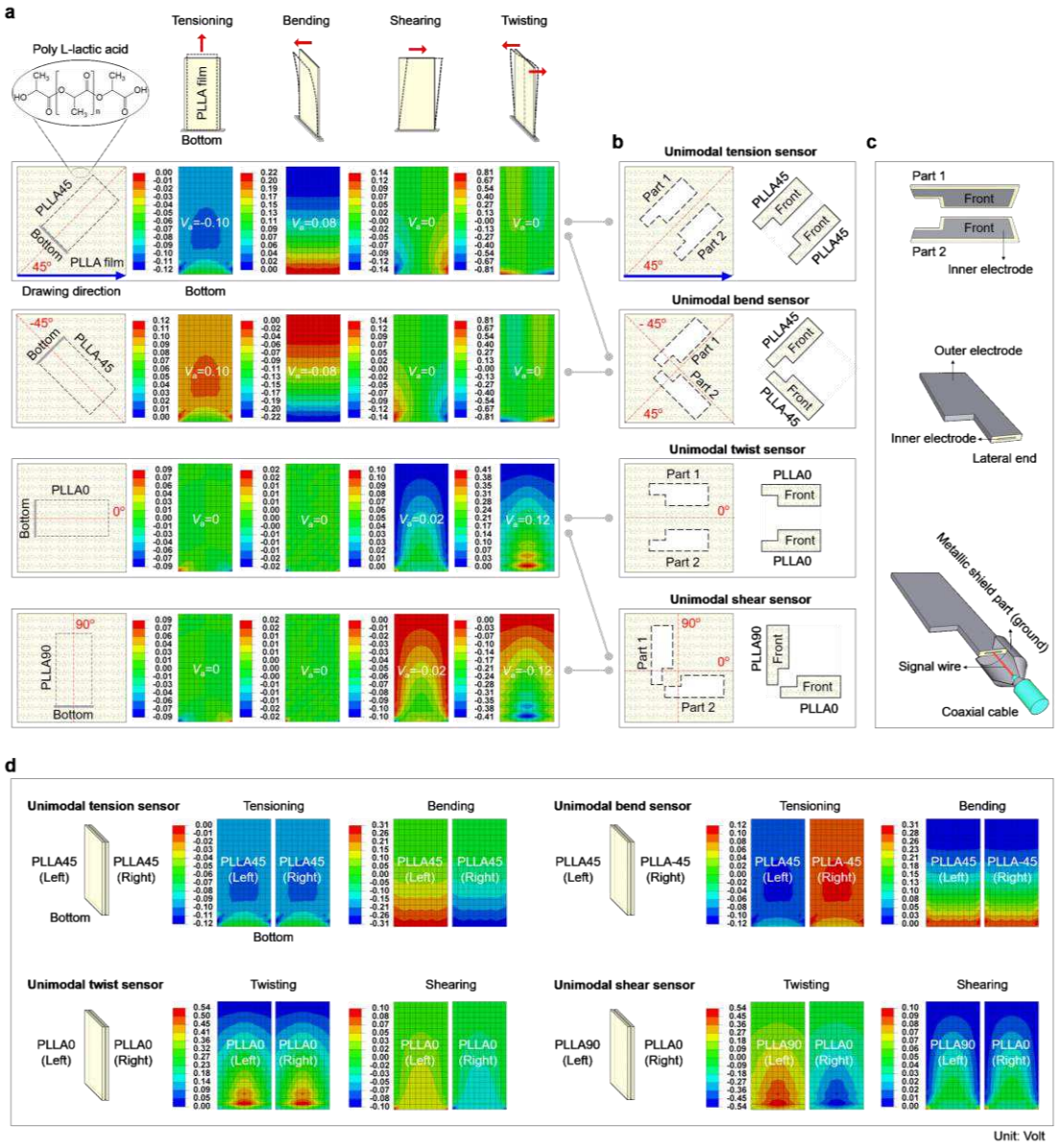

Fig. 1. Design concept of unimodal tension, bend, twist, and shear sensors. a, Top schematics show the applied forces and their directions (red arrows) for tensioning, bending, shearing, and twisting deformations in finite element simulations. The bottom panels show the piezoelectric response simulations of the uniaxially drawn piezoelectric PLLA films with different cutting angles under tensioning, bending, shearing, and twisting deformations. The first panel shows the uniaxially drawn piezoelectric PLLA film with a cutting angle of 45° (PLLA45 for short) and its cutting schematic (first graph) with a cutting shape (black dash line) and a cutting angle (red

dash line), and a PLLA molecular formula shown in the circle. The drawing direction (blue arrow) of the PLLA film is the same as the PLLA molecular chain's direction. The average responding voltage of all nodes of the PLLA film surface (V_a) is shown in the middle, and the PLLA film bottom is fixed when it is subject to tensioning, bending, shearing, and twisting forces. The same illustrative schemes are applied for PLLA-45, PLLA0, and PLLA90. **b**, Left schematics show the cutting angles (red dash lines) and cutting shapes (black dash line) of two parts from an original piezoelectric PLLA film for the unimodal tension, bend, twist, and shear sensors, respectively, and the right schematics show the corresponding parts after cutting out; **c**, Top schematic shows the patterns of inner electrodes (gray areas), and the front sides (i.e., inner electrodes) of two parts of each sensor are stuck together; the middle one shows the exposed area of each assembled sensor is coated with silver paste as an outer electrode, except the lateral end of the sensor; the bottom one shows the inner electrodes are connected to a signal wire, and the outer electrode is connected to a metallic shield part (ground) of a coaxial cable. **d**, Piezoelectric response simulations of two PLLA films composing each unimodal sensor under tensioning, bending, shearing, and twisting deformations to prove the unimodal sensors' hypothesis. The first panel shows the piezoelectric response of two PLLA45s of the unimodal tension sensor under tensioning and bending. The piezoelectric responses of the exposed areas of two PLLA45s are shown in simulation; in other words, the displayed voltages are on outer electrodes of the unimodal tension sensor. The generated voltages of the two PLLA45s are superimposed when tensioned, but they are offset under bending. The unimodal tension sensor under

422 twisting and shearing is not simulated because the PLLA45 is insensitive to the two
423 deformations, as demonstrated in Fig. 1a. The same illustrative schemes are applied for
424 the unimodal bend sensor under tensioning and bending, the unimodal twist sensor
425 under twisting and shearing, and the unimodal shear sensor under twisting and shearing.
426 Note that all parameters and applied forces used in these simulations (Fig. 1d) are the
427 same as the previous piezoelectric PLLA film simulations (Fig. 1a).
428
429
430
431
432
433
434
435
436
437
438
439

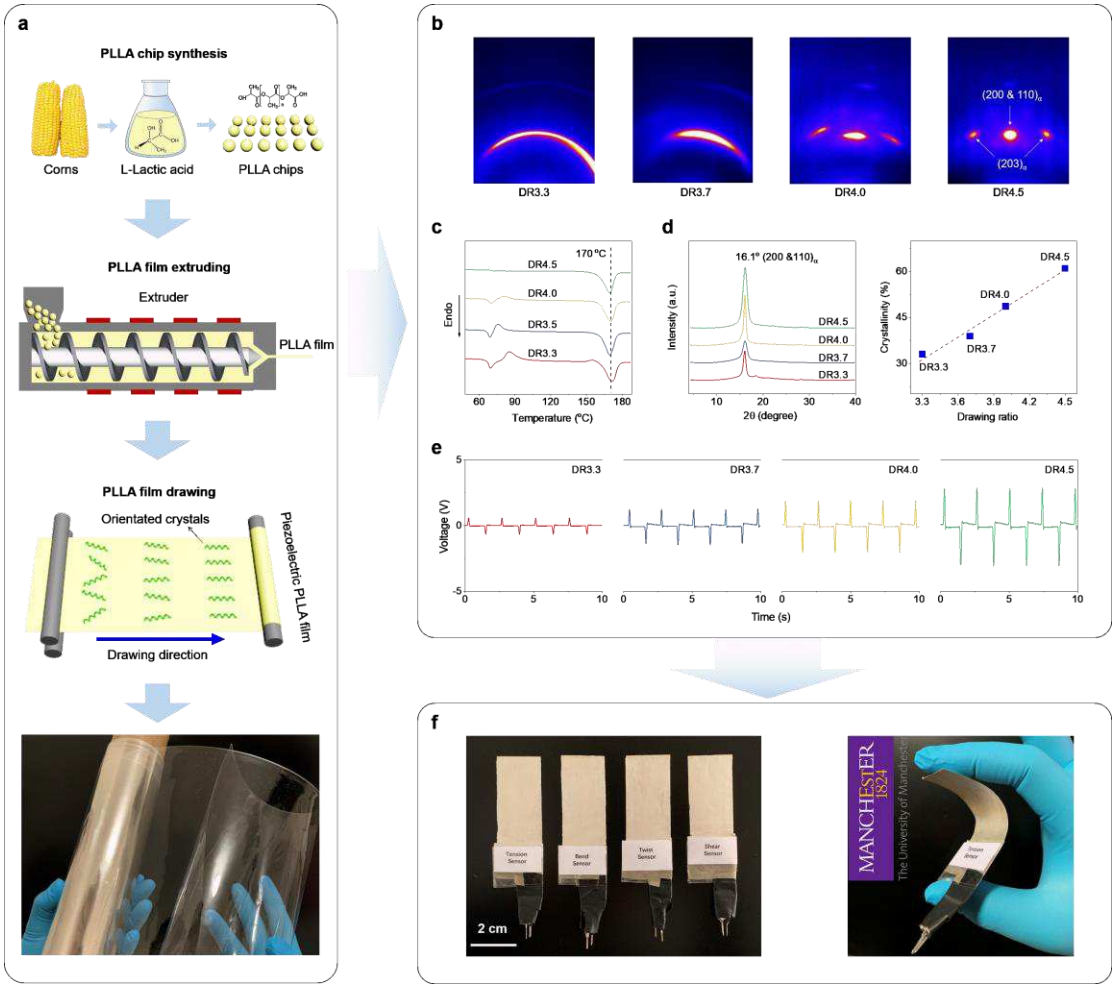

Fig. 2. Preparation and characterization of uniaxially drawn piezoelectric PLLA films. **a**, Schematic of uniaxially drawn piezoelectric PLLA films preparation process. The first photograph shows the PLLA chip synthesis, which is polymerized from L-lactic acid that is obtained from the fermentation of renewable and biodegradable plant sources such as corns[37]. In this work, we directly purchased the PLLA chips from NatureWorks, USA. The second photograph shows the PLLA film extruding. The PLLA chips are extruded into PLLA film at 225 °C using an extruder after dehumidifying at 120 °C under a vacuum for eight hours. The third photograph shows that PLLA film is stretched at different drawing ratios (DR) of 3.3, 3.7, 4.0, and 4.5 at 70 °C, and each sample names DR3.3, DR3.7, DR4.0, and DR4.5, respectively. The

bottom photograph shows a transparent piezoelectric PLLA film (DR4.5). **b**, Two-dimensional wide-angle x-ray diffraction (2D-WAXD) photographs of four PLLA film samples for crystal orientation analysis; **c**, Differential scanning calorimeter (DSC) melting thermograms of the PLLA films with different DRs for crystal form determination. **d**, 1D-WAXD spectrum of the PLLA films for crystal form determination (left) and their crystallinity (right). **e**, Comparison of piezoelectric response of four PLLA film samples under tensioning deformation. The dimension (Length × Width) of each sensor is 4 × 2 cm, and every PLLA film is cut at 45° from the drawing direction. **f**, Photographs of four unimodal sensors (left) and the sensor flexibility demonstration (right).

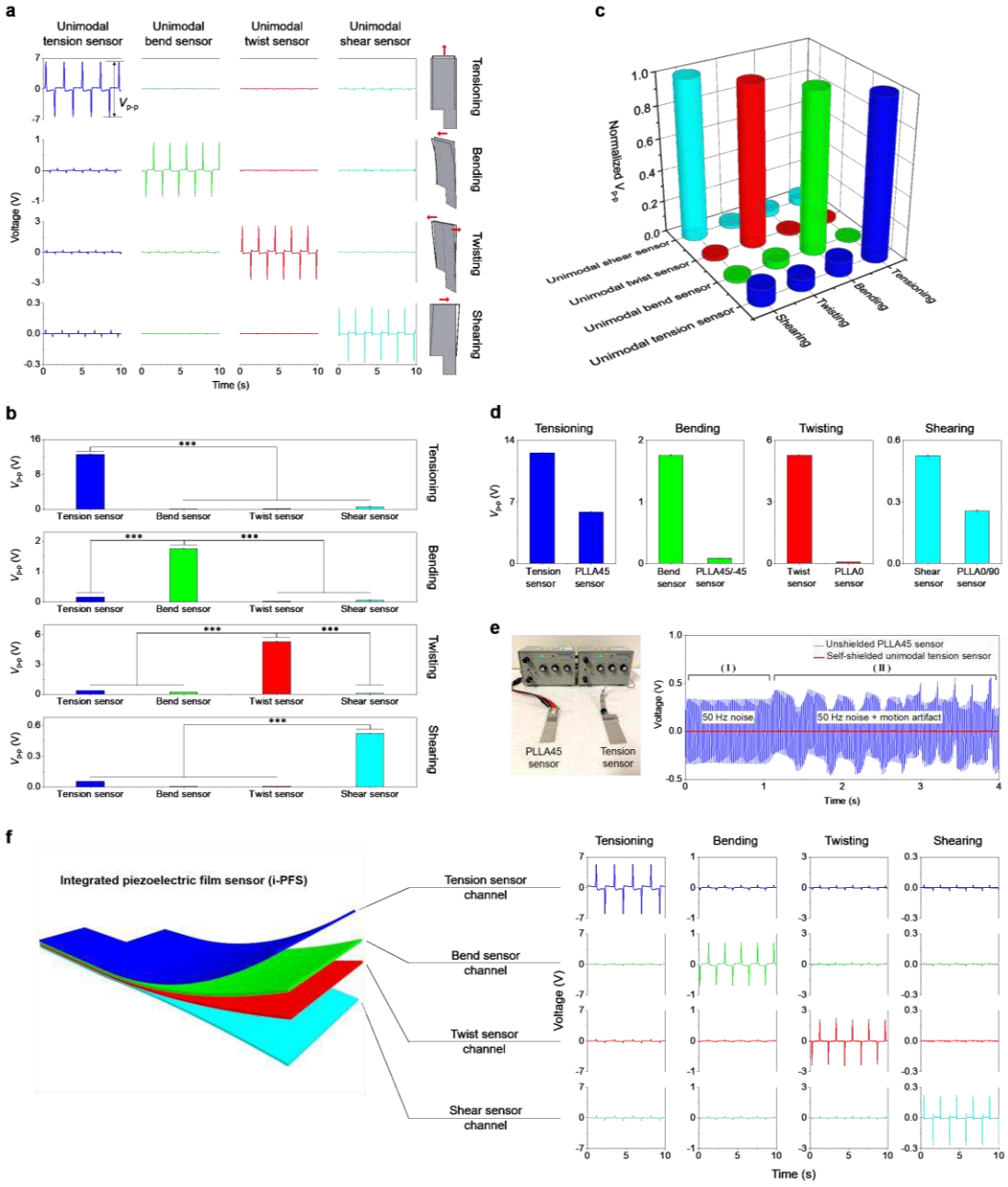

Fig. 3. Performance evaluation of four unimodal sensors and integrated piezoelectric film sensor (i-PFS). a, Piezoelectric responses of each unimodal sensor under the same tensioning, bending, twisting, and shearing conditions. Schematics of unimodal tension, bend, twist, and shear sensors with their corresponding deformations are shown in right insets. **b**, Comparison of the corresponding peak to peak signal amplitudes ($V_{p\text{-}p}$) of Fig. 3a (*** indicating P-value < 0.001). **c**, Normalized $V_{p\text{-}p}$ of

unimodal tension, bend, twist, and shear sensors under tensioning, bending, twisting, and shearing deformation conditions. **d**, Comparison of the piezoelectric response between the four unimodal sensors and the conventional single-layer PLLA sensors under the above conditions. **e**, The left photograph shows an experimental setup for the shielding performance test. The right figure shows the shielding performance of the unshielded PLLA45 sensor and the self-shielded unimodal tension sensor (I) under the static condition and (II) when walking/running next to two sensors. **f**, Schematic of the i-PFS comprising unimodal tension, bend, twist, and shear sensors (left). The right panels show the piezoelectric response of the i-PFS under the same tensioning, bending, twisting, and shearing conditions. All conditions are the same as those used for individual unimodal sensor (Fig. 3a).

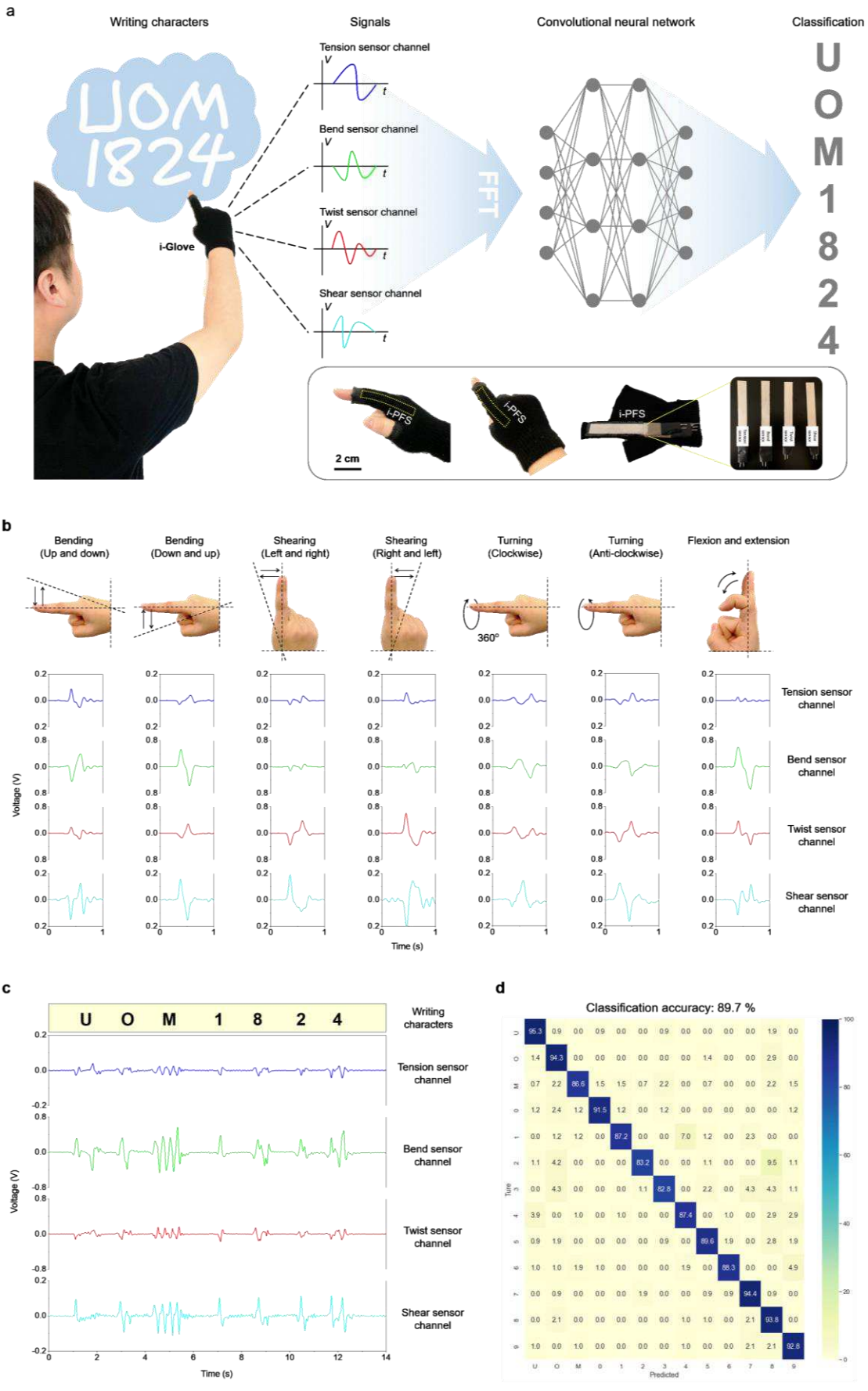

494

495 **Fig. 4. Demonstration of an i-PFS integrated glove (i-Glove) for finger-air-writing**

application. a, Schematic illustration of a finger-air-writing application. A participant wearing the i-Glove writes some characters, e.g., “U”, “O”, “M”, “1”, “8”, “2”, “4”, in the free space using his index finger. The four unimodal sensors of the i-PFS collect the corresponding signal of each character. The acquired signals are input into a pre-trained convolutional neural network (CNN) program after fast fourier transform (FFT). Finally, the program classifies the characters based on the signals. The bottom first two photographs show the i-PFS positions in the i-Glove at the side and top views. The third photograph shows the inside view of the i-Glove, in which the i-PFS is inserted into a transparent pocket of the index finger. The last photograph shows four unimodal sensors of the i-PFS. **b**, Index finger motion classification. Top photographs show index finger motions (bending, shearing, turning, and flexion and extension), and the bottom panels show corresponding raw output voltages from four unimodal sensor channels of the i-PFS. **c**, Top panel shows writing characters, and the bottom panel shows corresponding raw output voltages of four unimodal sensor channels of the i- PFS. **d**, Confusion matrix for the thirteen characters' classification accuracy and its mean accuracy (top) when using four unimodal sensor channels of the i-PFS.

References

1. Sundaram, S. *et al.* Learning the signatures of the human grasp using a scalable tactile glove. *Nature* **569**, 698–702 (2019).
2. Dong, W. *et al.* Soft human–machine interfaces: design, sensing and stimulation. *Int. J. Intell. Robot. Appl.* **2**, 313–338 (2018).
3. Song, K. *et al.* Pneumatic actuator and flexible piezoelectric sensor for soft virtual reality glove system. *Sci. Rep.* **9**, 1–8 (2019).
4. Kim, K. K. *et al.* A deep-learned skin sensor decoding the epicentral human motions. *Nat. Commun.* **11**, 1–8 (2020).
5. Boutry, C. M. *et al.* A stretchable and biodegradable strain and pressure sensor for orthopaedic application. *Nat. Electron.* **1**, 314–321 (2018).
6. Sun, T. *et al.* Decoding of facial strains via conformable piezoelectric interfaces. *Nat. Biomed. Eng.* **4**, 954–972 (2020).
7. Misra, S., Singha, J. & Laskar, R. H. Vision-based hand gesture recognition of alphabets, numbers, arithmetic operators and ASCII characters in order to develop a virtual text-entry interface system. *Neural Comput. Appl.* **29**, 117–135 (2018).
8. Mukherjee, S., Ahmed, S. A., Dogra, D. P., Kar, S. & Roy, P. P. Fingertip detection and tracking for recognition of air-writing in videos. *Expert Syst. Appl.* **136**, 217–229 (2019).
9. Homayounfar, S. Z. & Andrew, T. L. Wearable Sensors for Monitoring Human Motion: A Review on Mechanisms, Materials, and Challenges. *SLAS Technol.*

25, 9–24 (2020).

10. Stenlund, T. C. *et al.* Inter- and intra-tester reliability when measuring seated spinal postures with inertial sensors. *Int. J. Ind. Ergon.* **44**, 732–738 (2014).

11. Dagdeviren, C. *et al.* Recent progress in flexible and stretchable piezoelectric devices for mechanical energy harvesting, sensing and actuation. *Extrem. Mech. Lett.* **9**, 269–281 (2016).

12. Chorsi, M. T. *et al.* Piezoelectric Biomaterials for Sensors and Actuators. *Adv. Mater.* **31**, 1–15 (2019).

13. Dai, Y., Hu, H., Wang, M., Xu, J. & Wang, S. Stretchable transistors and functional circuits for human-integrated electronics. *Nat. Electron.* **4**, 17–29 (2021).

14. Wang, W. *et al.* Strain-insensitive intrinsically stretchable transistors and circuits. *Nat. Electron.* (2021). doi:10.1038/s41928-020-00525-1

15. Chen, L., Fu, J., Wu, Y., Li, H. & Zheng, B. Hand Gesture Recognition Using Compact CNN via Surface Electromyography Signals. *Sensors (Switzerland)* **20**, 672 (2020).

16. Moin, A. *et al.* A wearable biosensing system with in-sensor adaptive machine learning for hand gesture recognition. *Nat. Electron.* **4**, 54–63 (2021).

17. Collins, D. F., Refshauge, K. M., Todd, G. & Gandevia, S. C. Cutaneous receptors contribute to kinesthesia at the index finger, elbow, and knee. *J. Neurophysiol.* **94**, 1699–1706 (2005).

18. Burke, B. Y. D., Gandevia, S. C. & Macefield, G. Responses to passive

562 movement of receptors in joint, skin and muscle of the human hand. *J. Physiol.*
563 **402**, 347–361 (1988).
564 19. Tu, Y., Liu, L., Li, M., Chen, P. & Mao, Y. A review of human motion
565 monitoring methods using wearable sensors. *Int. J. Online Eng.* **14**, 168–179
566 (2018).
567 20. Huang, B. *et al.* Wearable stretch sensors for motion measurement of the wrist
568 joint based on dielectric elastomers. *Sensors (Switzerland)* **17**, (2017).
569 21. Cha, Y., Seo, J., Kim, J. S. & Park, J. M. Human-computer interface glove
570 using flexible piezoelectric sensors. *Smart Mater. Struct.* **26**, 5 (2017).
571 22. Araromi, O. A. *et al.* Ultra-sensitive and resilient compliant strain gauges for
572 soft machines. *Nature* **587**, 219–224 (2020).
573 23. Souri, H. *et al.* Wearable and Stretchable Strain Sensors: Materials, Sensing
574 Mechanisms, and Applications. *Adv. Intell. Syst.* **2**, 2000039 (2020).
575 24. Leber, A., Cholst, B., Sandt, J., Vogel, N. & Kolle, M. Stretchable
576 Thermoplastic Elastomer Optical Fibers for Sensing of Extreme Deformations.
577 *Adv. Funct. Mater.* **29**, 1–8 (2019).
578 25. Chander, H. *et al.* Wearable stretch sensors for human movement monitoring
579 and fall detection in ergonomics. *Int. J. Environ. Res. Public Health* **17**, 1–18
580 (2020).
581 26. Fukada, E. Recent developments of polar piezoelectric polymers. *IEEE Trans.*
582 *Dielectr. Electr. Insul.* **13**, 1110–1119 (2006).
583 27. Ando, M., Kawamura, H., Kageyama, K. & Tajitsu, Y. Film sensor device

584 fabricated by a piezoelectric poly(L-lactic acid) film. *Jpn. J. Appl. Phys.* **51**, 1–
585 4 (2012).
586 28. Curry, E. J. *et al.* Biodegradable Piezoelectric Force Sensor. *Proc. Natl. Acad.*
587 *Sci.* **115**, 909–914 (2018).
588 29. Ru, J. F. *et al.* Dominant β-form of poly(l -lactic acid) obtained directly from
589 melt under shear and pressure fields. *Macromolecules* **49**, 3826–3837 (2016).
590 30. Yin, H. M. *et al.* Effects of extrusion draw ratio on the morphology, structure
591 and mechanical properties of poly(L-lactic acid) fabricated using solid state
592 ram extrusion. *RSC Adv.* **5**, 69016–69023 (2015).
593 31. Atalay, A. *et al.* Batch Fabrication of Customizable Silicone-Textile Composite
594 Capacitive Strain Sensors for Human Motion Tracking. *Adv. Mater. Technol.* **2**,
595 1–8 (2017).
596 32. Curry, E. J. *et al.* Biodegradable nanofiber-based piezoelectric transducer.
597 *Proc. Natl. Acad. Sci. U. S. A.* **117**, 214–220 (2020).
598 33. Someya, T., Bao, Z. & Malliaras, G. G. The rise of plastic bioelectronics.
599 *Nature* **540**, 379–385 (2016).
600 34. Amma, C., Georgi, M. & Schultz, T. Airwriting: Hands-free mobile text input
601 by spotting and continuous recognition of 3d-space handwriting with inertial
602 sensors. *Proc. - Int. Symp. Wearable Comput. ISWC* 52–59 (2012).
603 doi:10.1109/ISWC.2012.21
604 35. Chen, M., AlRegib, G. & Juang, B. H. Air-Writing Recognition - Part I:
605 Modeling and Recognition of Characters, Words, and Connecting Motions.

606 *IEEE Trans. Human-Machine Syst.* **46**, 403–413 (2016).
607 36. Smith, M., Calahorra, Y., Jing, Q. & Kar-Narayan, S. Direct observation of
608 shear piezoelectricity in poly-l-lactic acid nanowires. *APL Mater.* **5**, (2017).
609 37. Muller, J., González-Martínez, C. & Chiralt, A. Combination Of Poly(lactic)
610 acid and starch for biodegradable food packaging. *Materials (Basel).* **10**, 1–22
611 (2017).

612 Acknowledgements

613 This work is financially supported by the EU Horizon 2020 through project
614 ETEXWELD-H2020-MSCA-RISE-2014 (Grant No. 644268) and the University of
615 Manchester through the UMRI project "Graphene-Smart Textiles E-Healthcare
616 Network" (Grant No. AA14512).

617 Author contributions

618 The work was conceived and designed by L.J., Y.L., and K.J.K. L.J. performed the
619 mathematical model and the piezoelectric response simulations and discussed them
620 with Y.L. and K.J.K. H.K. and K.J.K. prepared the uniaxially drawn piezoelectric PLLA
621 film. L.J. and L.X. supervised sensor fabrication. Z.L. and C.D. ran the piezoelectric
622 response test. Y.Z. assisted with the shielding performance test. H.Z. and P.Y. performed
623 the XRD experiment. L.J. and Q.S. fabricated the i-Sleeve and i-Glove. Z. L. and S.Q.X.
624 performed the CNN. L.J. drafted the manuscript, Y.L., K.J.K., S.Q.X, Z.L., and B.R.
625 revised the manuscript, and all authors discussed the results.

626 Competing financial interests

627 The authors declare no competing financial interests.

Materials & Correspondence

Correspondence and requests for materials should be addressed to Yi Li (henry.yili@manchester.ac.uk), Kap Jin Kim (kjkim@khu.ac.kr), and Sheng Q. Xie (S.Q.Xie@leeds.ac.uk).

Figures

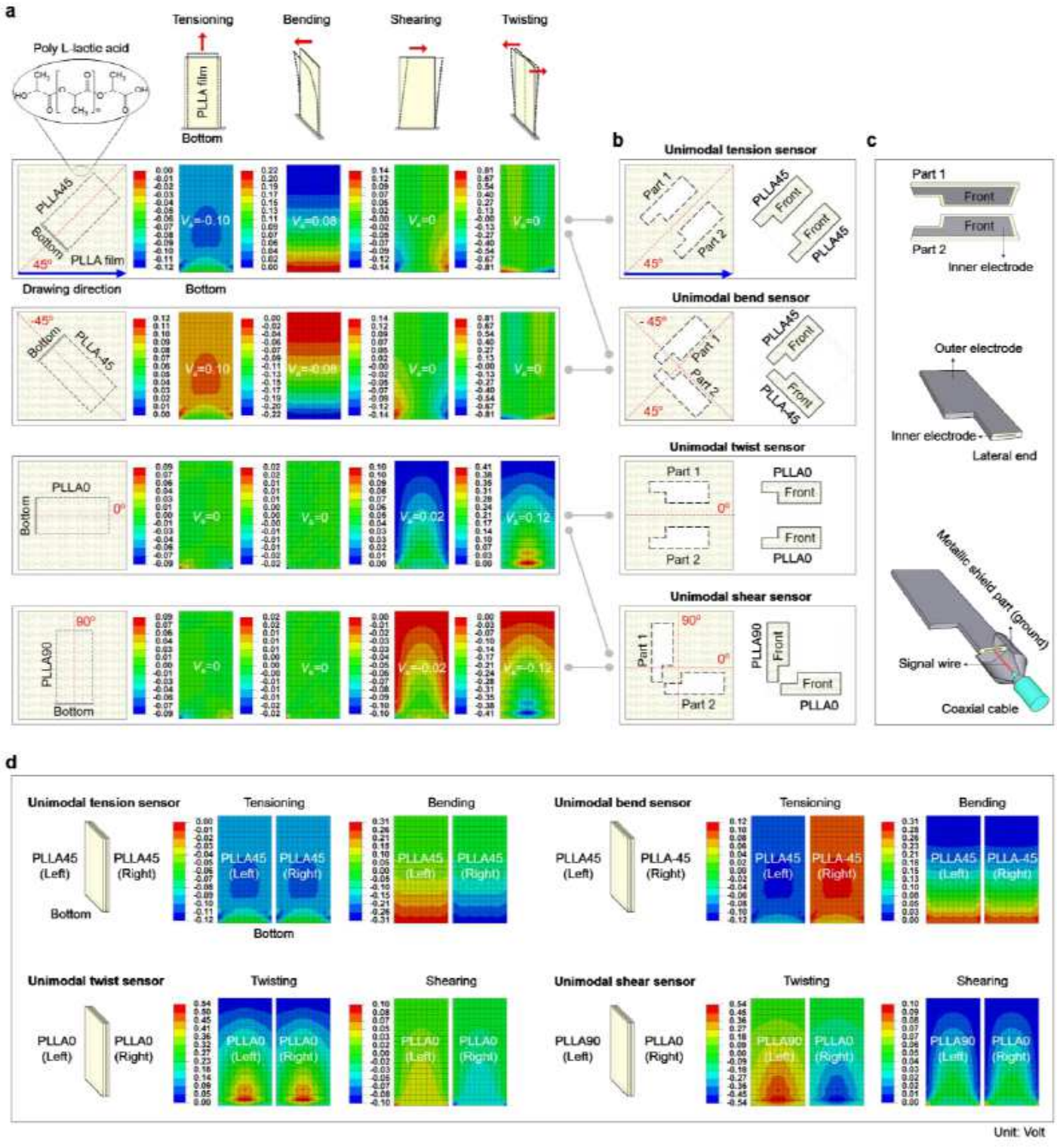

Figure 1

Design concept of unimodal tension, bend, twist, and shear sensors. a, Top schematics show the applied forces and their directions (red arrows) for tensioning, bending, shearing, and twisting deformations in finite element simulations. The bottom panels show the piezoelectric response simulations of the

uniaxially drawn piezoelectric PLLA films with different cutting angles under tensioning, bending, shearing, and twisting deformations. The first panel shows the uniaxially drawn piezoelectric PLLA film with a cutting angle of 45° (PLLA45 for short) and its cutting schematic (first graph) with a cutting shape (black dash line) and a cutting angle (red dash line), and a PLLA molecular formula shown in the circle. The drawing direction (blue arrow) of the PLLA film is the same as the PLLA molecular chain's direction. The average responding voltage of all nodes of the PLLA film surface (Va) is shown in the middle, and the PLLA film bottom is fixed when it is subject to tensioning, bending, shearing, and twisting forces. The same illustrative schemes are applied for PLLA-45, PLLA0, and PLLA90. b, Left schematics show the cutting angles (red dash lines) and cutting shapes (black dash line) of two parts from an original piezoelectric PLLA film for the unimodal tension, bend, twist, and shear sensors, respectively, and the right schematics show the corresponding parts after cutting out; c, Top schematic shows the patterns of inner electrodes (gray areas), and the front sides (i.e., inner electrodes) of two parts of each sensor are stuck together; the middle one shows the exposed area of each assembled sensor is coated with silver paste as an outer electrode, except the lateral end of the sensor; the bottom one shows the inner electrodes are connected to a signal wire, and the outer electrode is connected to a metallic shield part (ground) of a coaxial cable. d, Piezoelectric response simulations of two PLLA films composing each unimodal sensor under tensioning, bending, shearing, and twisting deformations to prove the unimodal sensors' hypothesis. The first panel shows the piezoelectric response of two PLLA45s of the unimodal tension sensor under tensioning and bending. The piezoelectric responses of the exposed areas of two PLLA45s are shown in simulation; in other words, the displayed voltages are on outer electrodes of the unimodal tension sensor. The generated voltages of the two PLLA45s are superimposed when tensioned, but they are offset under bending. The unimodal tension sensor under twisting and shearing is not simulated because the PLLA45 is insensitive to the two deformations, as demonstrated in Fig. 1a. The same illustrative schemes are applied for the unimodal bend sensor under tensioning and bending, the unimodal twist sensor under twisting and shearing, and the unimodal shear sensor under twisting and shearing. Note that all parameters and applied forces used in these simulations (Fig. 1d) are the same as the previous piezoelectric PLLA film simulations (Fig. 1a).

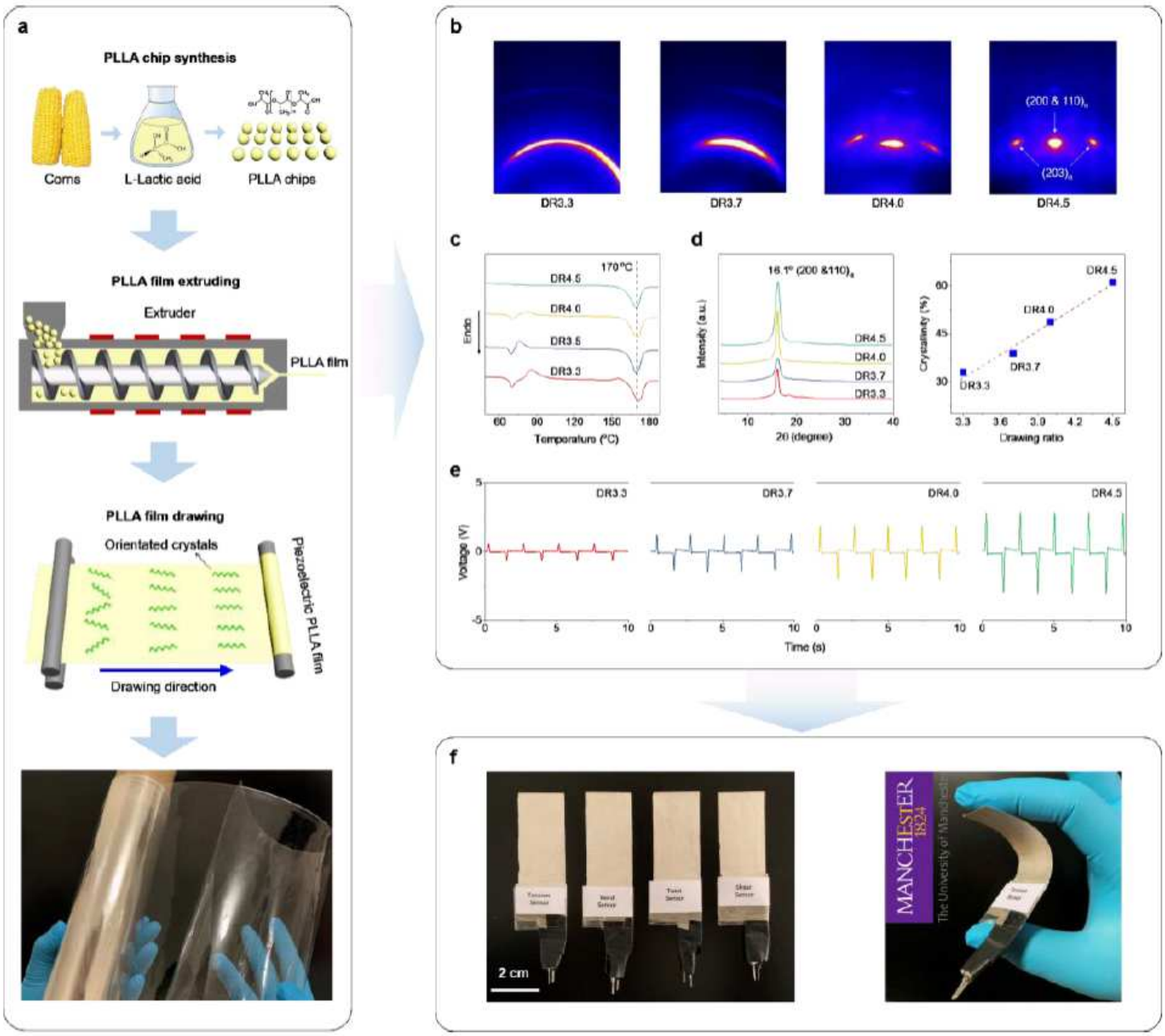

Figure 2

Preparation and characterization of uniaxially drawn piezoelectric PLLA films. a, Schematic of uniaxially drawn piezoelectric PLLA films preparation process. The first photograph shows the PLLA chip synthesis, which is polymerized from L-lactic acid that is obtained from the fermentation of renewable and biodegradable plant sources such as corns37. In this work, we directly purchased the PLLA chips from NatureWorks, USA. The second photograph shows the PLLA film extruding. The PLLA chips are extruded into PLLA film at 225 °C using an extruder after dehumidifying at 120 °C under a vacuum for eight hours. The third photograph shows that PLLA film is stretched at different drawing ratios (DR) of 3.3, 3.7, 4.0, and 4.5 at 70 °C, and each sample names DR3.3, DR3.7, DR4.0, and DR4.5, respectively. The bottom photograph shows a transparent piezoelectric PLLA film (DR4.5). b, Two-dimensional wide-angle x-ray

diffraction (2D-WAXD) photographs of four PLLA film samples for crystal orientation analysis; c, Differential scanning calorimeter (DSC) melting thermograms of the PLLA films with different DRs for crystal form determination. d, 1D-WAXD spectrum of the PLLA films for crystal form determination (left) and their crystallinity (right). e, Comparison of piezoelectric response of four PLLA film samples under tensioning deformation. The dimension (Length × Width) of each sensor is 4 × 2 cm, and every PLLA film is cut at 45° from the drawing direction. f, Photographs of four unimodal sensors (left) and the sensor flexibility demonstration (right).

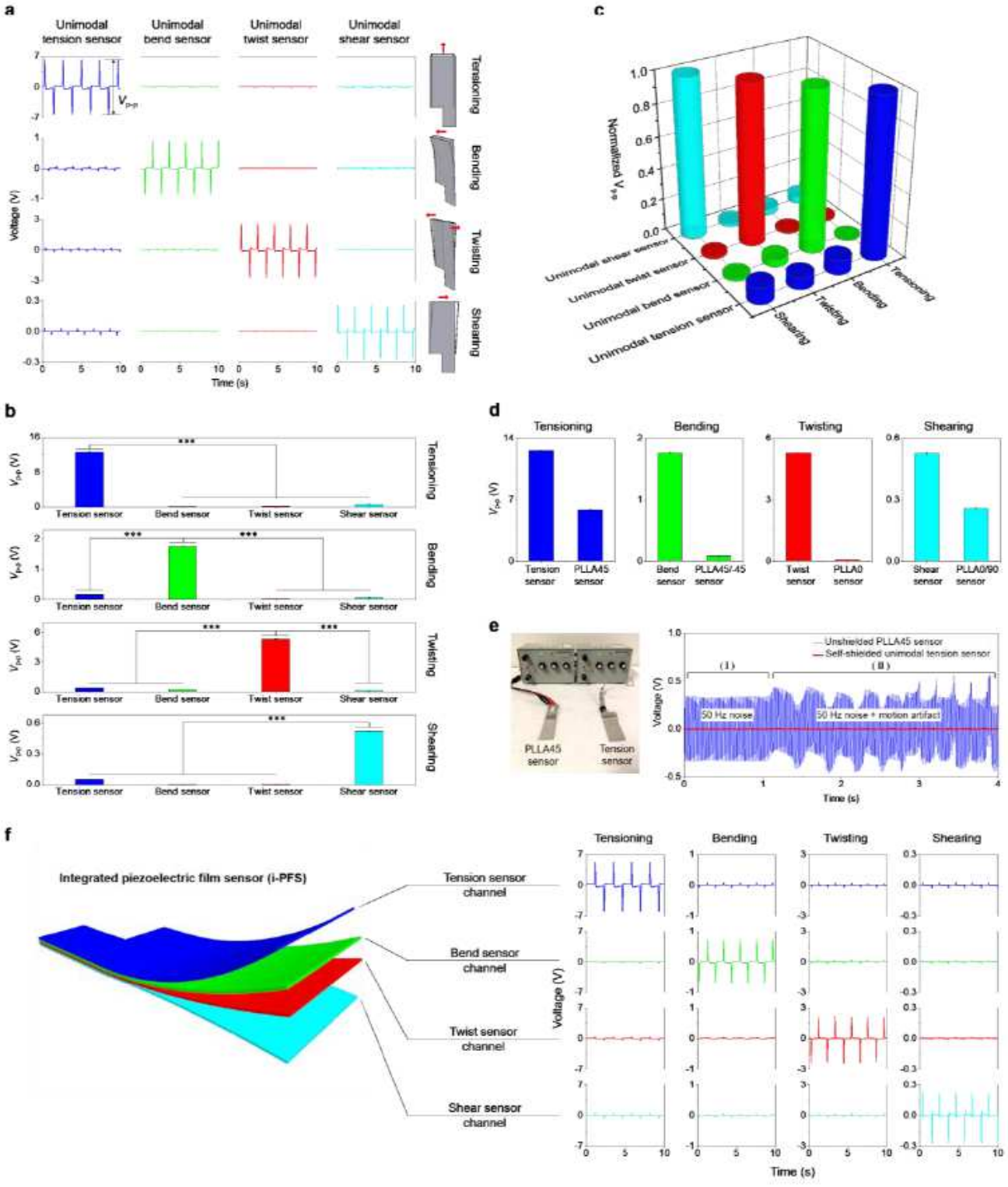

Figure 3

Performance evaluation of four unimodal sensors and integrated piezoelectric film sensor (i-PFS). a, Piezoelectric responses of each unimodal sensor under the same tensioning, bending, twisting, and shearing conditions. Schematics of unimodal tension, bend, twist, and shear sensors with their corresponding deformations are shown in right insets. b, Comparison of the corresponding peak to peak signal amplitudes (Vp-p) of Fig. 3a (*** indicating P-value < 0.001). c, Normalized Vp-p of unimodal tension, bend, twist, and shear sensors under tensioning, bending, twisting, and shearing deformation conditions. d, Comparison of the piezoelectric response between the four unimodal sensors and the conventional single-layer PLLA sensors under the above conditions. e, The left photograph shows an experimental setup for the shielding performance test. The right figure shows the shielding performance of the unshielded PLLA45 sensor and the self-shielded unimodal tension sensor (I) under the static condition and (II) when walking/running next to two sensors. f, Schematic of the i-PFS comprising unimodal tension, bend, twist, and shear sensors (left). The right panels show the piezoelectric response of the i-PFS under the same tensioning, bending, twisting, and shearing conditions. All conditions are the same as those used for individual unimodal sensor (Fig. 3a).

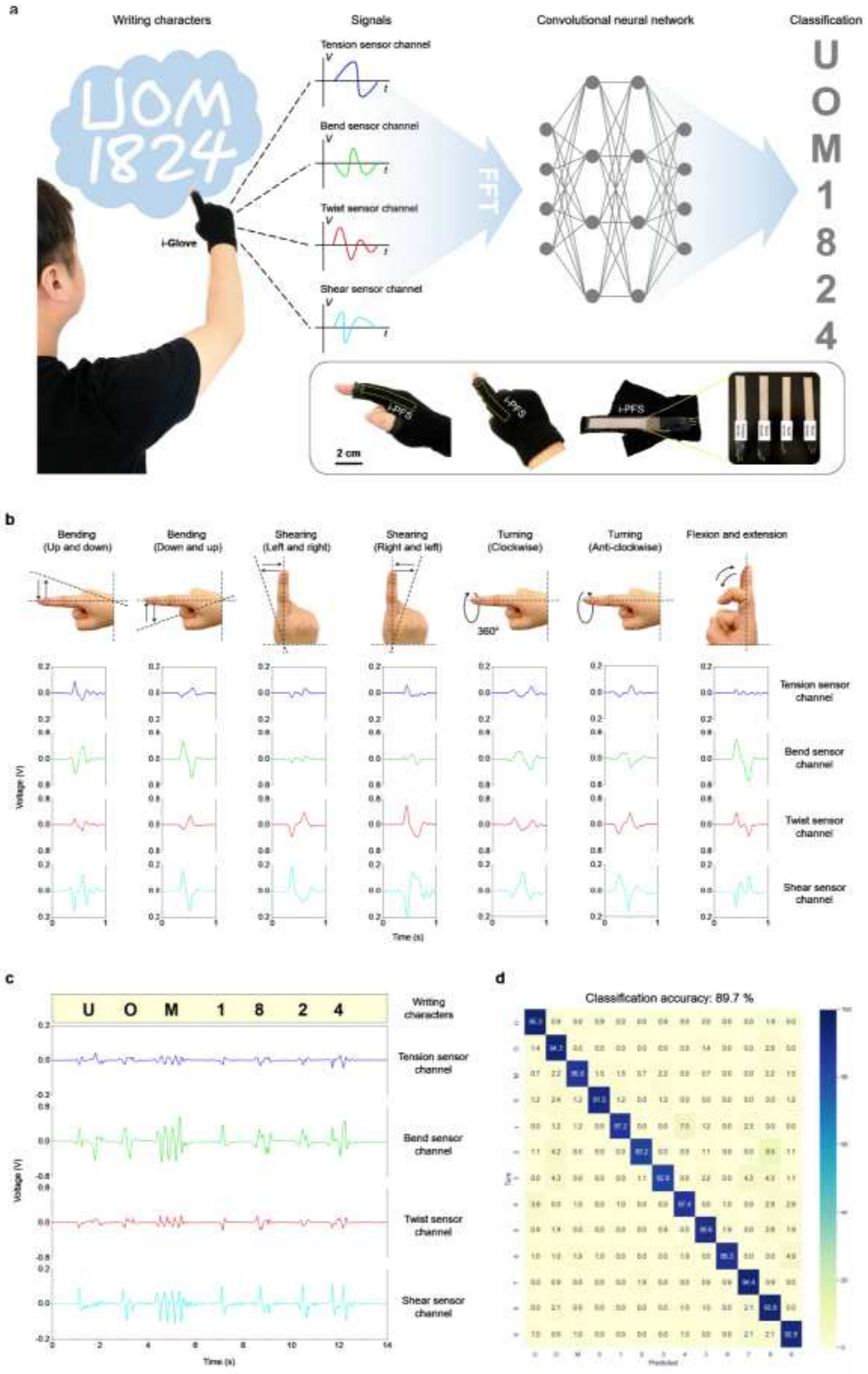

Figure 4

Demonstration of an i-PFS integrated glove (i-Glove) for finger-air-writing application. a, Schematic illustration of a finger-air-writing application. A participant wearing the i-Glove writes some characters, e.g., “U”, “O”, “M”, “1”, “8”, “2”, “4”, in the free space using his index finger. The four unimodal sensors of the i-PFS collect the corresponding signal of each character. The acquired signals are input into a pre-trained convolutional neural network (CNN) program after fast fourier transform (FFT). Finally, the

program classifies the characters based on the signals. The bottom first two photographs show the i-PFS positions in the i-Glove at the side and top views. The third photograph shows the inside view of the i-Glove, in which the i-PFS is inserted into a transparent pocket of the index finger. The last photograph shows four unimodal sensors of the i-PFS. b, Index finger motion classification. Top photographs show index finger motions (bending, shearing, turning, and flexion and extension), and the bottom panels show corresponding raw output voltages from four unimodal sensor channels of the i-PFS. c, Top panel shows writing characters, and the bottom panel shows corresponding raw output voltages of four unimodal sensor channels of the i- PFS. d, Confusion matrix for the thirteen characters' classification accuracy and its mean accuracy (top) when using four unimodal sensor channels of the i-PFS.

Supplementary Files

This is a list of supplementary files associated with this preprint. Click to download.

- Supplementaryinformation.pdf
- Video1forpiezoelectricresponsesimulationAnimationofFig1a.gif
- Video2forshieldingperformancetestunimodaltensionsensorandunshieldedPLLA45sensor.mp4
- Video3foriPFSdemonstration.mp4
- Video4foriSleevedemonstrationwristmotion.mp4
- Video5foriGlovedeomstrationfingerairwriting.mp4